GEOPHYSICAL RESEARCH LETTERS, VOL. 27, NO. 4, PAGES 581-584, FEBRUARY 15, 2000

The Waveguide Effect of Metastable Olivine in Slabs

Keith D. Koper

Dept. of Geosciences, University of Arizona, Tucson, AZ 85721

Douglas A. Wiens

Dept. of Earth and Planetary Sciences, Washington University, St. Louis, MO 63130

Abstract. We use a finite difference algorithm to compute *P-SV* synthetic seismograms for deep earthquakes recorded at regional seismic stations located above a subducting slab. We calculate synthetics for 2-D slab models in which the 410 km-discontinuity is uplifted, owing to the exothermic nature of the $\alpha \rightarrow \beta$ transition (the equilibrium model), and models in which the 410 km-discontinuity is depressed, owing to inhibited kinetics of the $\alpha \rightarrow \beta$ olivine transition (the metastable model). In the latter case the existence of the low-velocity wedge of metastable olivine has a profound influence on the waveforms of deep-focus earthquakes. The wedge acts as a geometrical waveguide, with the energy-focusing effect apparent even after the wavefront has traveled the several hundred kilometers from the wedge boundary to the Earth's surface. The guided energy is most pronounced for receivers located near the surface projection of the deep slab but is observable over a range of 300 km and so may provide a valuable diagnostic for discriminating between equilibrium and metastable models of subduction. A recent search for such guided energy, using regionally recorded *P* and *S* waves from deep events in Tonga, yielded negative results.

Introduction

The first-order seismic discontinuity observed globally at a depth of about 410 km is generally associated with the isochemical phase transition of silicate olivine (α) to the higher-pressure modified spinel structure (β, wadsleyite) [*Ringwood*, 1969; *Bina and Wood*, 1987]; however, the nature of this phase transition in the vicinity of subduction zones is subject to debate. It is thought that either (1) the discontinuity is uplifted within slabs because of their relatively cool temperatures and the exothermic nature of the $\alpha \rightarrow \beta$ transition or (2) the discontinuity is depressed because the cold slab temperatures inhibit the kinetics of the phase transition, allowing α to exist in a metastable state beyond the equilibrium depth of $\sim$ 410 km. Because the reaction kinetics are strongly temperature dependent, it is likely that only the coldest subducting lithosphere (e.g., in Tonga or Izu-Bonin) possesses metastable α, while equilibrium conditions are reached elsewhere (e.g., in Alaska or Cascadia). The determination of which model is correct, and where, is of great interest because the existence of a low-velocity, low-density wedge of metastable olivine has implications for the driving force of plate tectonics [*Schmeling et al.*, 1998; *Marton et al.*, 1999], the stress state of subducting lithosphere [*Goto et al.*, 1987; *Bina*, 1996], and the nucleation of deep-focus (> 350 km) earthquakes [*Green and Houston*, 1995; *Kirby et al.*, 1996].

Seismological investigations of this issue have concentrated on modeling *P*-wave travel times from deep and intermediate depth earthquakes [*Roecker*, 1985; *Iidaka and Suetsugu*, 1992; *Koper et al.*, 1998] and the analysis of mode conversions and reflections from the 410 km-discontinuity [*Vidale and Benz*, 1992; *Collier and Helffrich*, 1997; *Flanagan and Shearer*, 1998]. These studies have been either inconclusive or in favor of the equilibrium model, with the exception of *Iidaka and Suetsugu* [1992] who reported evidence for the existence of metastable α in the Izu-Bonin subduction zone.

The enhanced information contained in seismic waveforms is potentially more definitive than travel time studies alone. *Vidale et al.* [1991] calculated teleseismic synthetic waveforms for intermediate depth events in metastable olivine models and found that reflections off the wedge boundary can produce significant secondary arrivals (0 to 4 s after the direct wave) for certain ranges of take-off angle. These later arriving phases depend fundamentally on the existence of the metastable olivine wedge and do not exist for equilibrium slab models. Observations of such phases have not been reported, but it may require an ideal data set to discern the reflections [*Vidale et al.*, 1991]. Here we further investigate the possibility of exploiting waveform information by computing regional distance synthetic seismograms for deep-focus earthquakes. The effects of metastable olivine on seismic energy traveling updip are expected to be significant, hence characterization of such effects provides a powerful seismological tool for discriminating between equilibrium and metastable models of subduction.

Computation of Synthetic Seismograms

We calculate synthetic *P-SV* waveforms for 2-D equilibrium (uplifted 410 km-discontinuity) and metastable (depressed 410 km-discontinuity) models of subduction, with the 410 topography as the only difference between the simulations. The construction of the *P* velocity models, and the sensitivity of these models to the slab thermal structure and mineralogical parameters, is discussed in detail in *Koper et al.* [1998]. Here we use $dV_p/dT = -0.4\ ms^{-1}{}^{\circ}C^{-1}$, an effective Clapeyron slope of 3.0 $MPa^{\circ}C^{-1}$, a 700 $^{\circ}C$ isotherm for metastability, and a mantle that is 60% olivine. Our models are designed to simulate the Tonga subduction zone; in particular, the geometry of the Tonga slab includes a sharp

Paper number 1999GL011007.
0094-8276/00/1999GL011007$05.00

bend in the slab at $\sim$ 400 km depth (Figure 1). We generate corresponding S-wave and density models by scaling the P model by 0.54 and 0.4 $m^4 s^{-1} kg^{-1}$ respectively - values consistent with the average upper mantle [*Dziewonski and Anderson*, 1981].

We compute synthetic seismograms using a fourth-order, staggered grid, finite difference scheme, coded by A. Pitarka and based on the technique of *Vidale and Helmberger* [1988]. At each grid point in the velocity model horizontal and vertical displacement seismograms are calculated for a line source which extends to infinity in the direction normal to the 2-D grid. The criterion for numerical stability of this method is given as: $C_0 \delta t / h \leq \sqrt{3/8}$, where C_0 is the maximum seismic velocity, δt is the time step, and h is the spatial grid size [*Alford et al.*, 1974]. We use $\delta t = 0.05$ s and $h = 1.0$ km to satisfy this criterion, however numerical stability does not guarantee accurate calculations.

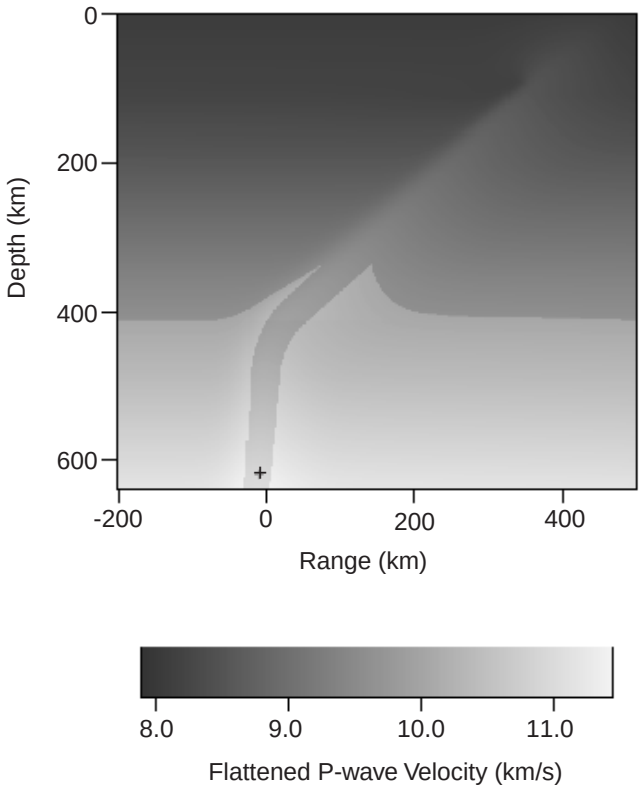

Figure 1. Metastable P velocity model of the subducting slab. The convergence rate, lithospheric age, and slab geometry have been chosen to simulate the Tonga slab. The velocities are shown having been altered by an Earth flattening transformation. The travel time errors introduced by using such a transformation on a 2-D model are negligible [*Koper et al.*, 1998]. The wedge thickness varies between 30 and 50 km, and across the phase transition the velocities and density increase by 4-5%. The black cross indicates the position of the source, which is placed at a depth of $\sim$ 600 km centered in the metastable wedge. The equilibrium velocity model is exactly the same except that the phase transition is uplifted to equilibrium conditions. In both cases we omit the crust and low velocity zone in the overlying mantle wedge to simplify the model comparison. For the calculations, we artificially expand the velocity models to the left (300 km), to the right (300 km), and downwards (510 km) so that energy which is reflected at the model boundaries does not interfere with the arrival of the P and SV waves.

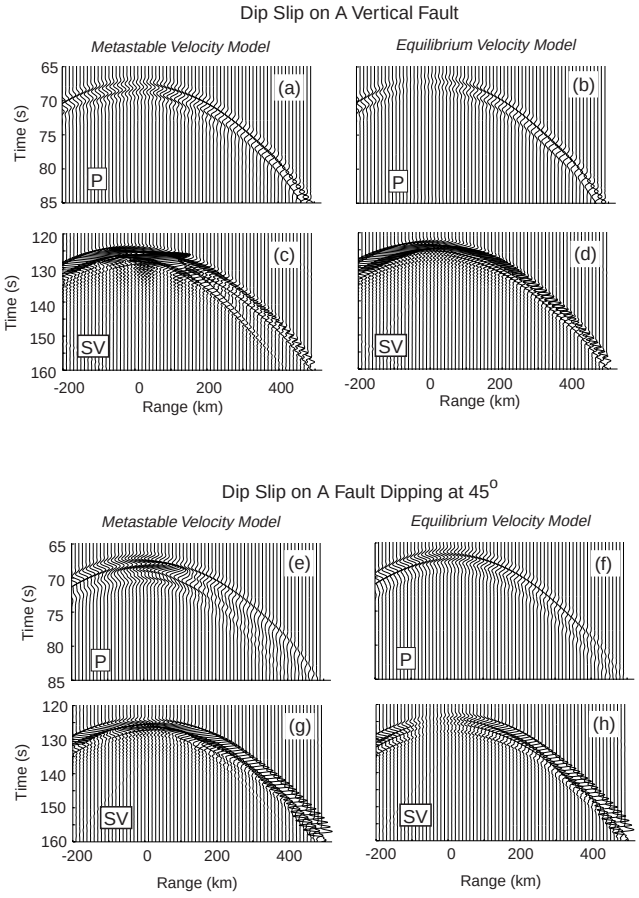

Figure 2. Displacement record sections for an array of 70 receivers spaced every 10 km at the surface. Shown on the left are (a) P waves and (c) SV waves for the metastable model using a vertical dip-slip focal mechanism, and (e) P waves and (g) SV waves for 45° dip-slip focal mechanism. The figures on the right (b,d,f,h) are the corresponding results for the equilibrium model. Note that the time scales for the P and SV waves differ. The computation does not include anelastic effects.

A significant source of error can arise when the dominant wavelength of the source pulse is small relative to h. This phenomenon is referred to as grid dispersion [*Alford et al.*, 1974] because the oscillatory ringing that characterizes it mimics the geometrical dispersion observed for the real Earth. We use the first derivative of a Gaussian function as the source pulse, with a peak-to-peak separation of 0.73 s. The upper half-power frequency of this source is 0.71 Hz, which gives at least 6 grid points per half-power wavelength ($G_0 \simeq 6$) for our simulations. With a fourth-order scheme good results are usually obtained with $G_0 > 5$ [*Alford et al.*, 1974].

Results

We place the source at a depth of 600 km, such that it is centered in the olivine wedge in the metastable model (Figure 1), and run the simulation for 4400 time steps (220 s). We convert the line-source synthetics to point source synthetics for two source geometries: dip slip on a vertical fault, which minimizes P (maximizes SV) amplitude directly above the source, and dip slip on a fault dipping at 45°, which has the opposite effect on P and SV ampli-

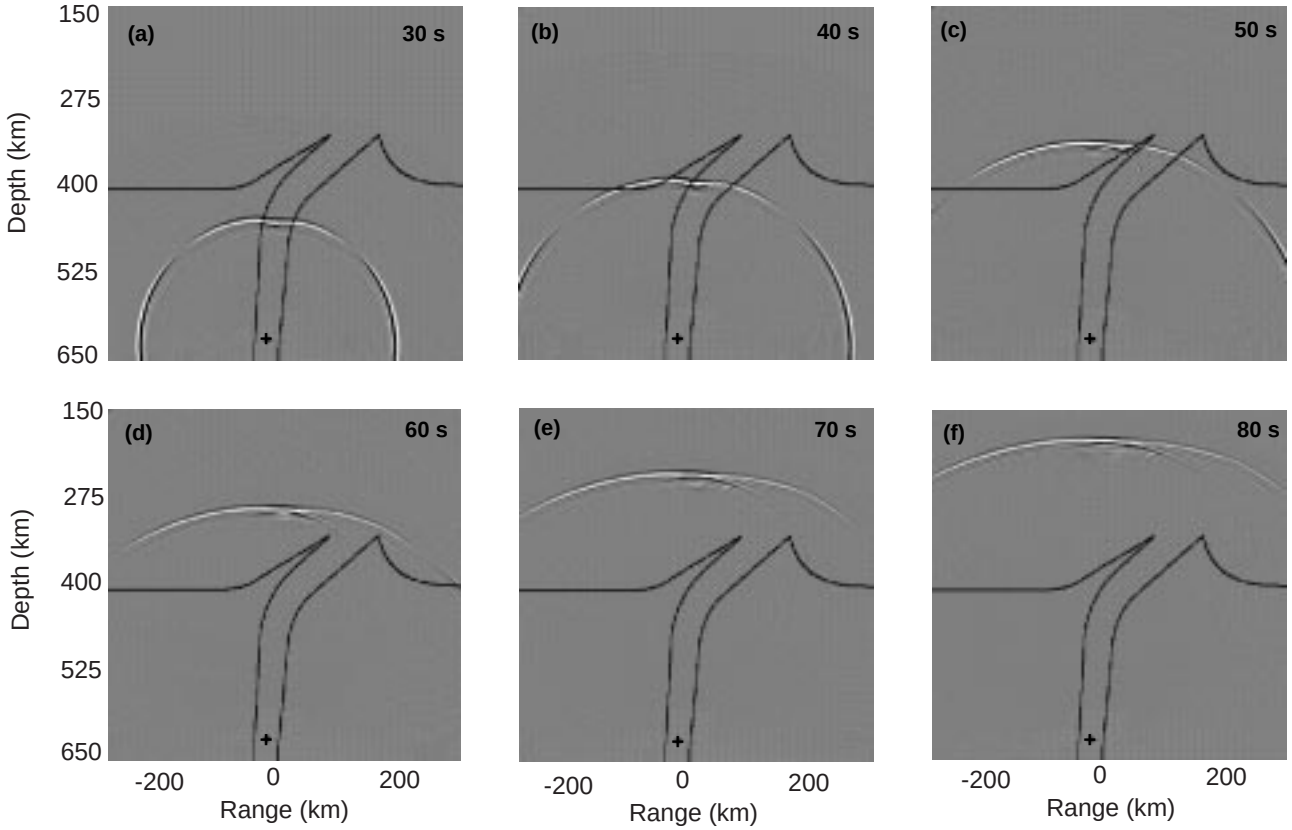

Figure 3. The curl of the displacement wavefield, near the wedge region, for the metastable model at (a) 30 s, (b) 40 s, (c) 50 s, (d) 60 s, (e) 70 s, and (f) 80 s. The curl operation eliminates compressional energy thus highlighting the SV waves. The guided energy is separated from the direct arrival by the curve of the olivine wedge. Similar results for P waves are seen when viewing the divergence of the wavefield.

tudes. These radiation patterns are chosen to maximize the waveform signature of the metastable olivine wedge.

The waveform signature of the metastable olivine wedge is dramatic: (1) both P and S energy are greatly enhanced at receivers near the surface projection of the wedge, to the point where the expected amplitude minima resulting from nodal planes are eliminated (Figures 2a,g), and (2) when seismic energy has a maximum directly above the source, a secondary phase is present after both the P and SV waves which is observable for a lateral range of ~ 300 km (Figures 2c,e). The anomalous energy observed for the metastable model is a consistent feature of the simulations and is unaffected by small changes in the grid size, δt, the source box dimensions, the length of the source time function, and the source coordinates.

To test the robustness of the calculations we compute synthetics in which the olivine content used in the metastable model is gradually decreased from 60% to 0%. In these simulations the amplitude of the later arriving energy decreases smoothly as the velocity contrast along the wedge boundaries is reduced, and becomes 0 for the case of no 410 km-discontinuity (0% olivine in the mantle). This strongly suggests that the energy is directly related to the depression of the $\alpha \rightarrow \beta$ transition and is not an artifact of the calculation. Furthermore, we compute synthetics for four additional metastable models in which we vary the P/S and P/ρ scaling relations by $\pm$ 10%; the appearance of the wedge induced energy is consistent in every case.

A final possibility is that the wedge-induced energy is caused by numerical error associated with grid dispersion. Given a source with a fixed frequency content, slower velocity models (i.e., metastable models) are more prone to yield waveforms contaminated by grid dispersion than faster velocity models (i.e., equilibrium models); similarly, SV waves are more susceptible to grid dispersion than P waves. We test our results presented in Figure 2 by computing synthetics for the wedge model using $h = 0.5$ km ($G_0 \simeq 12$). Owing to computational limitations the velocity grid must be confined to the dimensions shown in Figure 1, thus edge effects are apparent in the resulting synthetics. Nevertheless, the wedge-induced energy is virtually identical to that shown in Figure 2, whereas the grid dispersion of the SV waves (indicated by the oscillatory tails in Figure 2-d,h) is reduced by the smaller grid size.

Discussion

Since the waveguide effect of the metastable olivine appears similar for P and SV waves, it is likely that the seismic energy is being critically reflected in the low-velocity olivine wedge and that mode-conversion energy is insignificant. To investigate this we create 2-D wavefield visualizations of the finite-difference calculations (Figure 3). We calculate the divergence and the non-zero component of the curl vector for the displacement wavefield generated in the metastable model. The former minimizes the shear component of seis-

mic energy, while the latter minimizes the compressional component of seismic energy. The post-P energy is seen exclusively on the divergence plots, while the post-S energy is seen exclusively on the curl plots; in both cases this is true throughout the simulation. Thus, the anomalous guided energy is not due to $P - SV$ conversions along the wedge boundaries (i.e., is not a Stonely wave).

The wavefield visualizations also yield insight into the formation of the guided phases as distinct entities. As the wavefront initially propagates upward, the sole waveguide effect is the concentration of energy in the wedge interior (Figure 3a). The separation of this guided energy into a distinct phase does not occur until the wavefront encounters the curving wedge boundary (Figure 3b,c,d). Thus the change in dip of the slab is responsible for separating the guided energy from the direct arrivals. The increasing time lag of the guided phases is due to the increasing divergence between the ray paths taken by the direct energy and those taken by the guided energy which remains trapped in the low-velocity wedge. This interpretation is born out by further simulations: we find that as the dip of the deep part of the slab is gradually reduced to agree with the shallow dip, the move-out of the guided energy with respect to the direct energy is correspondingly reduced. In the case of a constant slab dip the guided energy does not separate from the direct energy and only appears as an enhanced amplitude and coda of the direct arrivals.

Conclusions

Synthetic seismogram calculations show that a wedge of metastable olivine has a profound effect on the regional waveforms of deep earthquakes. The presence of such a wedge causes the deep slab to act as a geometric waveguide, creating trapped energy which arrives after the direct P and S waves. The effect is most apparent for receivers located near the surface projection of the deep slab but is significant over a range of 300 km perpendicular to the strike of the subduction zone. The character of the guided energy is greatly influenced by the shape of the slab at depth. For a slab with a sharp increase in dip near the 410 km-discontinuity, such as in Tonga, the guided energy separates from the direct waves and becomes a coherent phase.

We have searched a data set consisting of regional waveforms from deep earthquakes in Tonga, recorded by a joint land-sea deployment of seismometers, and find no sign of guided energy after either the P or S waves. Taken with our previously reported travel time analysis of the Tonga data [*Koper et al.*, 1998], the results in this *Letter* imply that either (1) the signature of the metastable olivine wedge in Tonga is more subtle than predicted by our simplified 2-D models and is not seismologically resolvable, or (2) metastable olivine does not exist in a coherent wedge-like structure in Tonga.

Acknowledgments. We thank Arben Pitarka for making his finite difference waveform code available, and Dapeng Zhao for help with using it. We also thank John Vidale for discussions and cogent advice and Meredith Nettles for reviewing the manuscript. Finally, we thank Megan Flanagan and an anonymous referee for critical comments. This research was supported by the National Science Foundation under grants EAR9614502, EAR9712311, and EAR9805309.

References

Alford, R. M., K. R. Kelly, and D. M. Boore, Accuracy of finite-difference modeling of the acoustic wave equation, *Geophysics, 39*, 834-842, 1974.

Bina, C. R., Phase transition buoyancy contributions to stresses in subducting lithosphere, *Geophys. Res. Lett., 23*, 3563-3566, 1996.

Bina, C. R., and B. J. Wood, Olivine-spinel transitions: Experimental and thermodynamic constraints and implications for the nature of the 400-km seismic discontinuity, *J. Geophys. Res., 92*, 4853-4866, 1987.

Collier, J. D., and G. R. Helffrich, Topography of the "410" and "670" km seismic discontinuities in the Izu-Bonin subduction zone, *Geophys. Res. Lett., 24*, 1535-1538, 1997.

Dziewonski, A. M., and D. L. Anderson, Preliminary reference Earth model, *Phys. Earth Planet. Inter., 25*, 297-356, 1981.

Flanagan, M. P., and P. M. Shearer, Topography on the 410-km seismic velocity discontinuity near subduction zones from stacking of sS, sP, and pP precursors, *J. Geophys. Res., 103*, 21165-21182, 1998.

Goto, K., Z. Suzuki, and H. Hamaguchi, Stress distribution due to olivine-spinel phase transition in descending plate and deep focus earthquakes, *J. Geophys. Res., 92*, 13811-13820, 1987.

Green, H. W., and H. Houston, The mechanics of deep earthquakes, *Ann. Rev. Earth Planet. Sci., 23*, 169-213, 1995.

Iidaka, T., and D. Suetsugu, Seismological evidence for metastable olivine inside a subducting slab, *Nature, 356*, 593-595, 1992.

Kennett, B. L. N., and E. R. Engdahl, Traveltimes for global earthquake location and phase identification, *Geophys. J. Inter., 105*, 429-465, 1991.

Kirby, S. H., S. Stein, E. A. Okal, and D. C. Rubie, Metastable mantle phase transformations and deep earthquakes in subducting oceanic lithosphere, *Rev. Geophys., 34*, 261-306, 1996.

Koper, K. D., D. A. Wiens, L. M. Dorman, J. A. Hildebrand, and S. C. Webb, Modeling the Tonga slab: Can travel time data resolve a metastable olivine wedge?, *J. Geophys. Res., 103*, 30079-30100, 1998.

Marton, F. C., C. R. Bina, S. Stein, and D. C. Rubie, Effects of slab mineralogy on subduction rates, *Geophys. Res. Lett., 26*, 119-122, 1999.

Ringwood, A. E., Phase transformations in the mantle, *Earth and Planet. Sci. Lett., 5*, 401-412, 1969.

Roecker, S. W., Velocity structure in the Izu-Bonin seismic zone and the depth of the olivine-spinel phase transition in the slab, *J. Geophys. Res., 90*, 7771-7794, 1985.

Schmeling, H., R. Monz, and D. C. Rubie, The influence of olivine metastability on the dynamics of subduction, *Earth Planet. Sci. Lett., 165*, 55-66, 1998.

Toksöz, M. N., N. H. Sleep, and A. T. Smith, Evolution of the downgoing lithosphere and mechanisms of deep focus earthquakes, *Geophys. J. R. Astron. Soc., 35*, 285-310, 1973.

Vidale, J. E., and H. M. Benz, Upper-mantle seismic discontinuities and the thermal structure of subduction zones, *Nature, 356*, 678-683, 1992.

Vidale, J. E., and D. V. Helmberger, Elastic finite-difference modeling of the 1971 San Fernando, California earthquake, *Bull. Seism. Soc. Am., 78*, 122-141, 1988.

Vidale, J. E., Q. Williams, and H. Houston, Waveform effects of a metastable olivine tongue in subducting slabs, *Geophys. Res. Lett., 18*, 2201-2204, 1991.

Keith D. Koper, Dept. of Geosciences, University of Arizona, Tucson, AZ 85721. (e-mail: kkoper@geo.arizona.edu)

Douglas A. Wiens, Dept. of Earth and Planetary Sciences, Washington University, Campus Box 1169, One Brookings Dr., St. Louis, MO 63130. (e-mail: doug@kermadec.wustl.edu)

(Received August 25, 1999; revised November 3, 1999; accepted December 3, 1999.)